Mosaic Images Segmentation using U-net

Gianfranco Fenu[1][a], Eric Medvet[1][b], Daniele Panfilo[1], and Felice Andrea Pellegrino[1][c]

[1] *Dipartimento di Ingegneria e Architettura, Università degli Studi di Trieste, Trieste, Italy*

fenu@units.it, emedvet@units.it, fapellegrino@units.it, daniele.panfilo@phd.units.it

Keywords:
Cultural Heritage, Computer Vision, Deep Learning, Convolutional Neural Networks

Abstract:
We consider the task of segmentation of images of mosaics, where the goal is to segment the image in such a way that each region corresponds exactly to one tile of the mosaic. We propose to use a recent deep learning technique based on a kind of convolutional neural networks, called U-net, that proved to be effective in segmentation tasks. Our method includes a preprocessing phase that allows to learn a U-net despite the scarcity of labeled data, which reflects the peculiarity of the task, in which manual annotation is, in general, costly. We experimentally evaluate our method and compare it against the few other methods for mosaic images segmentation using a set of performance indexes, previously proposed for this task, computed using 11 images of real mosaics. In our results, U-net compares favorably with previous methods. Interestingly, the considered methods make errors of different kinds, consistently with the fact that they are based on different assumptions and techniques. This finding suggests that combining different approaches might lead to an even more effective segmentation.

1 Introduction and related works

Cultural heritage is one of the most important assets of the society. Its preservation and restoration are time-consuming activities performed by experts and often consist in manual analysis of fine details of the works. It is hence natural that these tasks, as many others where human experts are involved in some form of data processing, are subjected to automation using machine learning techniques. Differently than other domains, however, tasks concerning cultural heritage may be harder because of the scarcity of labeled data and nature of the data itself. Despite these limitations, successful examples of applications exist, e.g., (Assael et al., 2019), and progresses in the techniques for different kinds of data pave the way for other successful applications.

In this work we consider a particular kind of artistic works, i.e., mosaics. Mosaics are assemblies of small pieces of stone or similar materials, called *tiles* or tessellae, glued together with some binder or *filler*, such that the overall appearance of the assembly looks like a painting or some decorative pattern. Mosaics constitute an essential component of the cultural heritage for many (ancient) civilizations. Preservation, and, to some degree, restoration of mosaics might be enhanced if digital versions of the works were available. Moreover, the access to the artistic works might be eased using digital means, possibly as part of a process in which hard copies are obtained starting from digital copies, hence enlarging the portion of population that can access mosaics, regardless of their physical location (Neumüller et al., 2014). There have been a couple of approaches, namely (Youssef and Derrode, 2008; Bartoli et al., 2016), that proposed automatic methods for obtaining a digital version of the mosaic. All of them take as input an image of the mosaic, that can be cheaply obtained also for not-relocable mosaics, and output a *segmentation* of the image in which regions should correspond to tiles. Starting from the segmentation, a digital version of the mosaic may be obtained straightforwardly, hence easing the mosaic preservation and restoration and making it more accessible (Comes et al., 2014).

Here we propose a novel technique for mosaic

[a] https://orcid.org/0000-0003-0867-8388
[b] https://orcid.org/0000-0001-5652-2113
[c] https://orcid.org/0000-0002-4423-1666

image segmentation that is based on a recently proposed kind of convolutional neural networks (CNN), called U-net (Ronneberger et al., 2015). Our approach differs from the previous ones in the way the mosaic image is processed. The U-net processes the image at the pixel level, differently than the proposal by Bartoli et al. (2016), but permits, by design, that some pixels are not associated with any region, differently than the approach of Youssef and Derrode (2008): this means that using U-net for segmentation allows to model the presence of the filler. A key component of our approach is in the preprocessing phase that is part of the learning process: we propose a method for augmenting the dataset in such a way that the learning of U-net parameters is effective even when a small number of annotated examples are available. In facts, manual annotating mosaic images is a costly process (Bartoli et al., 2016).

We assess experimentally our approach applying it to 11 images of real mosaics, differing in style, age, and quality (both of the image and of the mosaic itself in terms of wear). We compare the segmentation based on U-net against previous methods using a set of established performance indexes suitable for the mosaic image segmentation task and we found that our method outperforms the other ones in the most relevant index. Moreover, we show that the way in which the three methods make errors in analyzing the image varies consistently with the fact that the methods are based on different underlying assumptions. This finding opens an opportunity for designing an even more effective method where U-net segmentation is a step of a more complex procedure which involves also other processing steps, eventually resulting in a better segmentation effectiveness.

Despite the availability of a “digital model” could be very useful, in the literature only few segmentation algorithms have been proposed, taking into account the specific structure features of a mosaic, i.e., shape, organisation, color of tiles, and the presence of the filler. In particular, in (Youssef and Derrode, 2008) the proposed approach aims to detect and to extract the tile from the filler, using the well-known watershed algorithm (Vincent and Soille, 1991) and some mosaic-specific preprocessing. In (Bartoli et al., 2016) the authors proposal goal is the same, but they employed *deformable models* as flexible shapes to be superimposed on the mosaic picture and to be adapted to the effective shapes of the tiles. The optimization of such deformable shapes has been performed by means of a genetic algorithm.

In addition to these approaches, many other techniques have been applied with the aim to obtain a digital model of a mosaic: among others laser scanners and photogrammetry (Fazio et al., 2019), segmentation based on already available mosaic cartoons (Monti and Maino, 2011). We refer the reader to (Benyoussef and Derrode, 2011) for a detailed review.

Regarding the U-nets, there are many applications in biomedical image segmentation, e.g., (Falk et al., 2019). Variations of the U-nets have also been applied to volumetric segmentation from sparsely annotated volumetric images (Çiçek et al., 2016), road extraction from aerial images (Zhang et al., 2018), and in case of ambiguous images, i.e., when many different annotations are available for every single image (Kohl et al., 2018).

2 Problem statement

The goal of this work is to propose a method for segmenting an image of a mosaic in such a way that, for each tile of the mosaic in the image, all and only the corresponding pixels are assigned to the same region of the segmentation.

More formally, we call a *region* of the image I a subset of adjacent pixels of I. We call a *segmentation* of an image I a set $\mathcal{T} = \{T_1, \dots, T_n\}$ of disjoint regions of I, i.e., $\forall i, j, T_i \cap T_j = \emptyset$.

Let $\mathcal{T}$ and $\mathcal{T}'$ be two segmentations of the same image I. Accordingly to (Fenu et al., 2015), we define the following three indexes:

$$\mathrm{Prec}(\mathcal{T}, \mathcal{T}') = \frac{1}{|\mathcal{T}|} \sum_{T \in \mathcal{T}} \max_{T' \in \mathcal{T}'} \frac{|T \cap T'|}{|T|} \tag{1}$$

$$\mathrm{Rec}(\mathcal{T}, \mathcal{T}') = \frac{1}{|\mathcal{T}'|} \sum_{T' \in \mathcal{T}'} \max_{T \in \mathcal{T}} \frac{|T \cap T'|}{|T'|} \tag{2}$$

$$\mathrm{Fm}(\mathcal{T}, \mathcal{T}') = 2 \frac{\mathrm{Prec}(\mathcal{T}, \mathcal{T}')\mathrm{Rec}(\mathcal{T}, \mathcal{T}')}{\mathrm{Prec}(\mathcal{T}, \mathcal{T}') + \mathrm{Rec}(\mathcal{T}, \mathcal{T}')} \tag{3}$$

$$\mathrm{Cnt}(\mathcal{T}, \mathcal{T}') = \frac{\mathrm{abs}(|\mathcal{T}'| - |\mathcal{T}|)}{|\mathcal{T}'|} \tag{4}$$

where $|T|$ is the number of pixels in the region T, $|\mathcal{T}|$ is the number of regions in the segmentation $\mathcal{T}$, and $T \cap T'$ is the set of pixels which belong to both T and T'.

The *precision* index $\mathrm{Prec}(\mathcal{T}, \mathcal{T}')$ is the average precision of regions in $\mathcal{T}$, where the precision of a region T is the largest ratio $\frac{|T \cap T'|}{|T|}$ among different $T' \in \mathcal{T}'$, i.e., the proportion of T pixels which belong to the region of $\mathcal{T}'$ with which T overlaps most. The *recall* index $\text{Rec}(\mathcal{T}, \mathcal{T}')$ is the average recall of regions in $\mathcal{T}'$, where the recall of a region T' is the largest ratio $\frac{|T \cap T'|}{|T'|}$ among different $T \in \mathcal{T}$, i.e., the proportion of T' pixels which belong to the region of $\mathcal{T}$ with which T' overlaps most—it can be noted that $\text{Prec}(\mathcal{T}, \mathcal{T}') = \text{Rec}(\mathcal{T}', \mathcal{T})$. The *F-measure* (also known as F-1 score) is the harmonic mean of *precision* and *recall*. Finally, the *count error* index $\text{Cnt}(\mathcal{T}, \mathcal{T}')$ is the normalized absolute difference between the number of regions in $\mathcal{T}'$ and the number of regions in $\mathcal{T}$.

It can be seen that, when the indexes are applied to the same segmentation, $\text{Prec}(\mathcal{T}, \mathcal{T}) = 1$, $\text{Rec}(\mathcal{T}, \mathcal{T}) = 1$, and $\text{Cnt}(\mathcal{T}, \mathcal{T}) = 0$. Intuitively, the more similar the two segmentations $\mathcal{T}$ and $\mathcal{T}'$, the closer the precision and recall indexes to 1 and the closer the count error index to 0. In the extreme case where $\mathcal{T} = \{I\}$, i.e., $\mathcal{T}$ consists of a single region covering the full image, recall is 1, whereas precision may be low and count error may be high; on the opposite case, if $\mathcal{T} = \{\{i\} : i \in I\}$, i.e., if regions of $\mathcal{T}$ correspond to single pixels of I, then precision is 1, recall may be low, and count error may be high.

Let $\mathcal{T}^\star$ be the unknown *desired segmentation* of a mosaic image I in which each region exactly corresponds to a tile in the image. The goal is to find a method that, for any image I of a mosaic, outputs a segmentation $\mathcal{T}$ which maximizes $\text{Prec}(\mathcal{T}, \mathcal{T}^\star)$ and $\text{Rec}(\mathcal{T}, \mathcal{T}^\star)$ and minimizes $\text{Cnt}(\mathcal{T}, \mathcal{T}^\star)$.

3 U-net for mosaic segmentation

We propose a solution for the mosaic image segmentation problem described in the previous section which is based on a kind of Convolutional Neural Network (CNN). We assume that a *learning set* composed of images of mosaics and the corresponding desired segmentations are available. In a *learning phase*, to be performed just once, the learning set is used to learn the values of the parameters of the network. Then, once learned, the network is used in a procedure that can take any image I as input and outputs a segmentation $\mathcal{T}$.

The CNN used in this study is known as U-net, the name deriving from the shape of the ANN architecture. U-net was introduced by Ronneberger et al. (2015) who used it for the segmentation of neuronal structures in electron microscopic stacks: according to the cited study, U-net experimentally outperformed previous approaches.

When applied to an image, a U-net works as a binary classifier at the pixel level, i.e., it takes as input a 3-channels (RGB) image and returns as output a two-channels image. In the output image, the two channels correspond to the two classes and encodes, together, the fact that the pixel belongs or does not belong to the artifact of interest—in our case, a tile of the mosaic.

In order to obtain a segmentation from the output of the U-net, we (i) consider the single-channel image that is obtained by applying pixel-wise the softmax function to the two channels of the ANN output and considering just the first value, that we call the *pixel intensity* and denote by $p(i)$; (ii) compare each pixel intensity against a threshold τ; (iii) merge sets of adjacent pixels that exceed the threshold, hence obtaining connected regions. We discuss in detail this procedure in Section 3.2.

Internally, the U-net is organized as follows: a contracting path made of a series of 3×3 unpadded convolutions followed by max-pooling layers enables the context capturing while the expanding path consisting of transposed convolutions and cropping operations ensures precise features localization (Ronneberger et al., 2015).

In our study we used an instance of the U-net tailored to input images of 400×400. In the contracting path, we used two 2-D un-padded convolutions steps of size 3, both made of 32 filters and followed by a rectified linear unit (reLU) precede a max-pooling layer with 2×2 pool-size. The same structure is repeated four times every time increasing the number of filters to 64, 128, 256, and 512. At the end of the contraction phase the 400×400 pixels input image in reshaped in a 17×512 tensor. In the expansion path, we started with an up-sampling 2-D layer of 2×2 size of the features map followed by a concatenation with the correspondingly cropped feature map from the contracting phase and two 2-D un-padded convolutions steps of size 3×3 each with reLU activation function. The same procedure is repeated also four times every time reducing the number of convolutions filter by half leading to a tensor of shape 216×32. Furthermore a zero-padding 2-D layer reshapes the tensor in a $400 \times 400 \times 32$ shape prior to a 1-D convolution steps composed of two filters that gives in output a $400 \times 400 \times 2$ tensor that constitutes the output of the U-net. The output is then used to compute pixel intensities and hence the segmentation as briefly sketched above and detailed in Section 3.2.

3.1 Learning

Let $L = \{(I_1, \mathcal{T}_1^\star), \dots, (I_m, \mathcal{T}_m^\star)\}$ be the learning set composed of m pairs, each consisting of a mosaic image I_i and the corresponding desired segmentation $\mathcal{T}_i^\star$, obtained by manual annotation. The outcome of the learning phase consists of the weights $\boldsymbol{\theta}$ of the U-net.

We first preprocess the pairs in the learning set L as follows, obtaining a different learning set L', for which $|L'| = |L|$ does not generally hold.

1. We rescale each pair $(I, \mathcal{T}^\star) \in L$ so as to obtain a given *tile density* $\rho_0 = \frac{|\mathcal{T}^\star|}{|I|}$, i.e., a given ratio between the number of tiles in the image and the image size; ρ_0 is a parameter of our method. We use a bicubic interpolation over 4×4 pixel neighborhood.
2. From each pair $(I, \mathcal{T}^\star) \in L$, we obtain a number of pairs by cropping square regions of I of size $l \times l$ (*crops*) that overlap for half of their size; l is a parameter of our method. Let $w \times h$ be the size of the image I of the pair, the number of pairs obtained by cropping is $\left(\lfloor \frac{w}{l} \rfloor + \lfloor \frac{w}{l} - \frac{1}{2} \rfloor\right)\left(\lfloor \frac{h}{l} \rfloor + \lfloor \frac{h}{l} - \frac{1}{2} \rfloor\right)$. We build a set L' including the resulting pairs, each one consisting of a square image of size $l \times l$ and a segmentation with, on average, approximately $\rho_0 l^2$ regions.
3. Finally, we augment L' by adding, for each of its pair, few pairs obtained by common image data augmentation techniques, i.e., rotation, horizontal and vertical flipping.

We remark that, when building L' from L, segmentations $\mathcal{T}^\star$ are processed accordingly to the processing of the corresponding images I.

In order to learn the weights $\boldsymbol{\theta}$ of the U-net, we consider a subset L'_train of L' that contains 90% of the pairs in L', chosen with uniform probability.

Then, we use the Adam optimizer (Kingma and Ba, 2015) on image pairs in L'_train to learn the weights $\boldsymbol{\theta}$. We feed Adam with batches of 8 images and drive it by the following weighted binary cross entropy loss function:

$$\begin{aligned}\text{Loss}(\boldsymbol{\theta}) = &-\frac{1}{|L_\text{b}|} \sum_{I \in |L_\text{b}|} \sum_{i \in I} \Big(w q(i) \log p(i) \\ &+ (1 - q(i)) \log(1 - p(i)) \Big) \end{aligned} \quad (5)$$

where L_b is the batch of pairs $(I, \mathcal{T}^\star)$, w is a weighting factor, $p(i)$ is the pixel intensity of i obtained by applying the U-net with weights $\boldsymbol{\theta}$, and $q(i)$ is an indicator function that encodes in $\{1, 0\}$ the fact that the pixel i belongs or does not belong to a region of $\mathcal{T}^\star$:

$$q(i) = \begin{cases} 1 & \text{if } \exists T \in \mathcal{T}^\star, i \in T \\ 0 & \text{otherwise} \end{cases} \quad (6)$$

We use the weighting factor w in Equation (5) in order to weight differently classification errors for pixels of tiles and filler. The parameter w hence permits to cope with the fact that image of mosaics are in general highly unbalanced: much more pixel are associated to tiles than to the filler. We experimented with three different values of w: 0.5, 0.1, and 0.01, the former corresponding to weighting the two classes equally.

We set Adam to run the optimization for n_epoch epochs, with a learning rate that varies at every epoch using an exponential decay function. During the optimization, we use the remaining 10% of the set L' for monitoring the progress, by computing the loss of Equation (5) on $L' \setminus L'_\text{train}$.

3.2 Segmentation

In the segmentation phase, we use a learned U-net to obtain a segmentation $\mathcal{T}$ out of an image I, as follows.

1. We rescale the input image such that its estimated tile density ρ is approximately equal to the ρ_0 value used during the learning. For computing ρ, and hence for performing the scaling, we assume that a raw estimate of the number of tiles in the image I is available: in practice, this estimate might be obtained by visual inspection of a small portion of the image.
2. We apply the U-net to I obtaining a single-channel image of pixel intensities that we threshold at 0.5, hence obtaining a binary image of the same size of I. We call this image the *output mask*.
3. We consider the subset $I' = \{i \in I, p(i) \geq 0.5\}$ of pixels of I that are classified by the U-net as a belonging to tiles.
4. Finally, we partition I' in subsets composed of adjacent pixels, hence obtaining the segmentation $\mathcal{T} = \{T_1, T_2, \dots\}$.

4 Experimental evaluation

We performed an extensive experimental evaluation aimed at assessing our method effectiveness in terms of precision, recall, and count error on images of mosaics not used for learning. To this end, we considered a set of images of real mosaics, that we manually annotated to obtain the corresponding desired segmentations (i.e., the *ground-truth* segmentations), and applied our method.

We collected a dataset of 12 images of real mosaics including both images that we acquired with a consumer camera and images that we obtained online. Part of this dataset has already been used by Bartoli et al. (2016).

The mosaics depicted in the images of our dataset belong to different ages in time and also differ in tile density and color. The annotation required for the training was performed manually. Despite the extensive effort and attention devoted to the process, some dissimilarities between a mosaic image and its corresponding ground-truth segmentation may still exist. Nonetheless, the manually annotated mask looks visually correct.

Figure 1 shows the images of our dataset. It can be seen that the images greatly vary in the density and size of the tiles as well as in the visually perceived sharpness of tile edges.

4.1 Procedure

We evaluated our method using a *leave-one-out* procedure on the images (and corresponding desired segmentations) of our dataset, as follows. For each pair $(I, \mathcal{T}^\star)$ in the dataset D, we (i) performed the learning on $L = D \setminus (I, \mathcal{T}^\star)$, hence obtaining a learned U-net, (ii) used the learned U-net for obtaining the segmentation $\mathcal{T}$ of I (i.e., the image of the left-out pair), and (iii) computed the precision $\text{Prec}(\mathcal{T}, \mathcal{T}^\star)$, recall $\text{Rec}(\mathcal{T}, \mathcal{T}^\star)$, and count error $\text{Cnt}(\mathcal{T}, \mathcal{T}^\star)$.

Concerning the method parameters, we set $\rho_0 = 15 \times 10^{-5}$, $l = 400$, and $n_\text{epoch} = 10$. We chose the values for ρ_0 and l based on the minimum dimension and tile density of the images in our dataset. In this way we obtained crops of 400×400 pixels with approximately $l^2\rho_0 = 24$ tiles in each crop. In the segmentation phase, we set $\rho = \rho_0$ and computed ρ using the actual number $\mathcal{T}^\star$ of tiles.

We run the experiments using an implementation of the method based on Python 3.6 with Keras and Tensorflow; we executed it on some p3.8xlarge AWS EC2 instances, each equipped with 64 vCPU based on 2.3 GHz Intel Xeon E5-2686 v4 with 244 GB RAM and with 4 GPUs based on NVIDIA Tesla V100 with 32 GB RAM. In these settings, the learning time for one repetition of a leave-one-out procedure is 30 min and the segmentation time is in the order of few seconds.

4.2 Results and discussion

We show in Table 1 the results in terms of the salient segmentation effectiveness indexes presented in Section 2 (precision, recall, F-measure, and count error) for each mosaic image, i.e., each repetition of the leave-one-out procedure.

Table 1 shows that average precision, recall, and F-measure at $w = 0.5$ are 0.60, 0.70, and 0.64 respectively, whereas the average count error is 0.36. By looking at the figures of single images, it can be seen that the effectiveness of segmentation varies among mosaic images, with the F-measure ranging from 0.51 of image 2 to 0.73 of image 7 and the count error ranging from 0.75 of image 2 to 0.15 of image 4. We carefully compared the numerical features of Table 1 with the corresponding mosaic images (see Figure 1) and found that the segmentation effectiveness is consistent with the subjectively perceived quality of the images. Good numerical results are obtained by our method for images 7 and 11, while the worst result is obtained for image 2 which exhibits poor sharpness.

Concerning the impact of the weighting parameter w, it can be seen from the three sections of Table 1 that it act consistently with its semantic. As w decreases, the balancing between precision and recall varies, namely precision increases and recall decreases: in facts, a lower value for w corresponds to a lower contribution, in the loss used during the learning (see Equation (5)), of the errors in classifying pixel belonging to the actual tiles. As a result, the learned U-net tends to outputs smaller regions that have a lower recall and a greater precision. Another effect is that the count error is lower with lower values of w, because there are fewer regions of the output segmentation in which tiles are "glued" together (see also later discussion). These finding on the impact of w on the output segmentations suggests that it can be used as a parameter to tailor the output to the specific usage intended by the user. However, since in our experiments $w = 0.5$ delivers the best F-measure, we report in the following

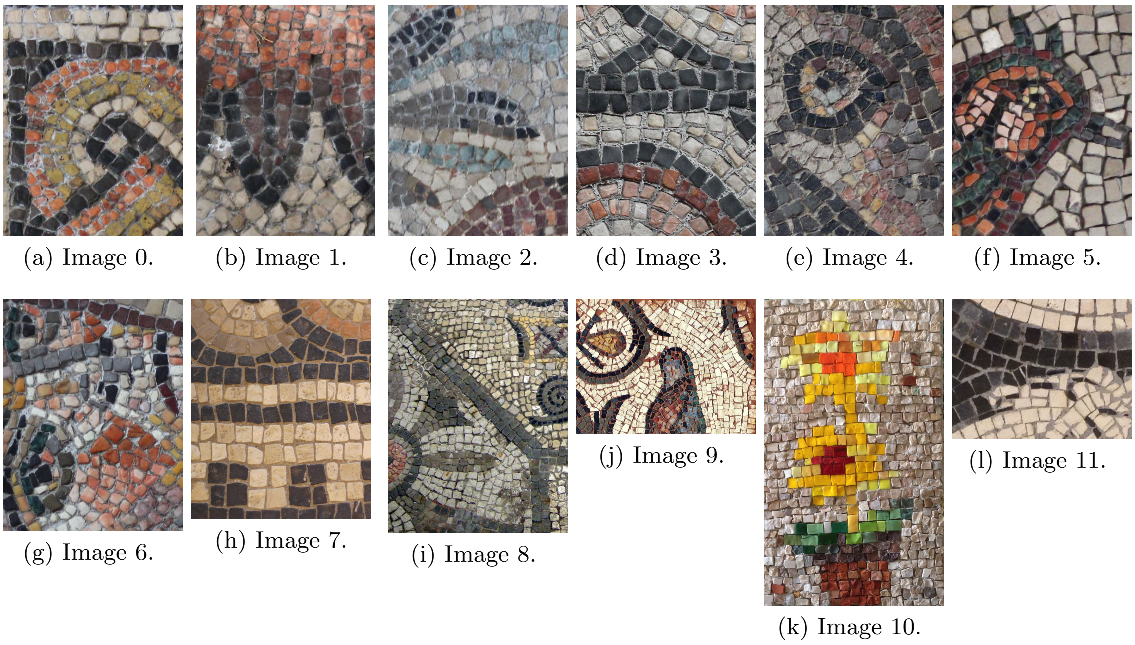

(a) Image 0. (b) Image 1. (c) Image 2. (d) Image 3. (e) Image 4. (f) Image 5.

(g) Image 6. (h) Image 7. (i) Image 8. (j) Image 9. (k) Image 10. (l) Image 11.

Figure 1: The images of the dataset. Images from 7 to 11 has been used also in Bartoli et al. (2016); Fenu et al. (2015).

	U-net with $w = 0.5$				U-net with $w = 0.1$				U-net with $w = 0.01$			
Im. #	Cnt	Prec	Rec	Fm	Cnt	Prec	Rec	Fm	Cnt	Prec	Rec	Fm
0	0.49	0.56	0.71	0.62	0.18	0.62	0.54	0.57	0.19	0.74	0.40	0.51
1	0.52	0.57	0.69	0.62	0.20	0.70	0.56	0.61	0.19	0.81	0.30	0.43
2	0.75	0.41	0.76	0.51	0.40	0.51	0.52	0.51	0.40	0.51	0.40	0.43
3	0.18	0.64	0.73	0.68	0.07	0.79	0.67	0.72	0.17	0.96	0.35	0.51
4	0.15	0.66	0.61	0.64	0.10	0.68	0.57	0.62	0.08	0.79	0.38	0.51
5	0.31	0.66	0.62	0.64	0.26	0.68	0.57	0.62	0.21	0.86	0.23	0.36
6	0.32	0.58	0.61	0.59	0.17	0.63	0.60	0.61	0.11	0.81	0.32	0.46
7	0.30	0.67	0.80	0.73	0.26	0.73	0.76	0.75	0.41	0.73	0.70	0.71
8	0.28	0.59	0.71	0.64	0.29	0.62	0.67	0.64	0.27	0.68	0.53	0.59
9	0.21	0.62	0.73	0.67	0.23	0.67	0.60	0.62	0.13	0.73	0.52	0.60
10	0.52	0.65	0.70	0.67	0.41	0.70	0.62	0.65	0.31	0.88	0.31	0.45
11	0.29	0.65	0.72	0.69	0.25	0.68	0.68	0.68	0.24	0.83	0.23	0.35
Avg.	0.36	0.60	0.70	0.64	0.23	0.67	0.61	0.63	0.22	0.78	0.39	0.49

Table 1: Results obtained with the three U-nets with different w values.

only the results obtained in this settings.

4.2.1 Comparison with other methods

In order to put our results in perspective, we compared them with those obtained by the two other existing methods for mosaic image segmentation, i.e., (Bartoli et al., 2016) and (Youssef and Derrode, 2008), that we here denote by GA and TOS, respectively. Table 2 shows the values of the four indexes for the mosaic images of our dataset which were also processed with GA and TOS (for these methods, the figures are taken from (Bartoli et al., 2016)). For each image, we highlight in Table 2 the best Fm and Cnt figure among the three methods.

The foremost finding is that our method outperforms both GA and TOS in terms of average F-measure, with 0.67 vs. 0.54 and 0.66, respectively: considering Fm on the single images, our method obtains the best result in 3 on 5 images.

	U-net with $w = 0.5$				GA				TOS			
Im. #	Cnt	Prec	Rec	Fm	Cnt	Prec	Rec	Fm	Cnt	Prec	Rec	Fm
7	0.30	0.67	0.80	0.73	**0.03**	0.50	0.76	0.60	0.14	0.64	0.87	**0.74**
8	0.28	0.59	0.71	**0.64**	**0.03**	0.42	0.63	0.50	0.54	0.56	0.72	0.63
9	0.21	0.62	0.73	**0.67**	**0.01**	0.41	0.66	0.51	0.03	0.53	0.82	0.64
10	0.52	0.65	0.70	**0.67**	0.07	0.50	0.63	0.56	**0.06**	0.49	0.68	0.57
11	0.29	0.65	0.72	0.69	**0.03**	0.46	0.67	0.55	0.90	0.63	0.78	**0.70**
Avg.	0.32	0.64	0.73	0.68	0.03	0.46	0.67	0.54	0.33	0.57	0.77	0.66

Table 2: Results obtained with our method and with GA and TOS for a subset of the dataset.

Concerning the count error, U-net scores better than TOS (0.30 vs. 0.33) and worse than GA (0.30 vs. 0.03): we note, however, that the latter method is designed to output a number of tiles corresponding to the user-provided estimate.

Another finding concerns how the errors in segmentation are distributed between precision and recall. For all the three methods, recall is in general larger than precision, meaning that tiles in the computed segmentation are in general "larger" than the corresponding tiles in the desired segmentation. The unbalancing is, however, much greater in TOS and GA than in U-net, the difference between recall and precision being 0.09, 0.21, and 0.20 respectively for our method, GA and TOS. We think that this difference can be explained by the way the three methods work. In TOS, the segmentation does not allow to obtain regions which are not tiles: this means that the filler is always included in a tile, resulting in a low precision and good recall. In GA, the overlapping of tiles is not explicitly forbidden or discouraged, thus the precision is very low, on average, because the output segmentation often contains tiles which span across many desired tiles. In our method, instead, the network is trained to discriminate between pixels belonging or not belonging to a tile in the desired segmentation: the way the loss is computed during the training of the U-net (see Equation (5)) favors a good balancing between false positive and false negative classification at the level of pixels and, hence, between precision and recall.

In Figure 2 we compare the visual results of the segmentation of image 11 using the three methods. Due to the aforementioned differences between the algorithms, the number of tiles in the TOS segmentation is higher while the size of the tiles tend to be smaller when compared to the other methods. In GA, since the algorithm allows for tiles overlapping, many of the predicted tiles share the same area. In the U-net segmentation some tiles are not properly separated, however position, size, and count are visually closer to those in the original image.

5 Conclusions and future work

We considered the problem of the segmentation of mosaic images and proposed a method based on deep learning, namely U-net. We experimentally evaluated our proposal on a set of 11 images of real mosaics acquired in different conditions, with different image quality, and with different building properties. The results suggest that our method is effective, scoring the better value for the most relevant index on the majority of images used in the comparison.

We think that our results constitute a further evidence that modern deep learning systems can help solving tasks in a variety of fields, here in digital humanities.

We believe that further improvements in mosaic image segmentation might be obtained. The most promising way to achieve them might be merging together two radically different techniques: the one presented in the present paper, based on deep learning, and the one designed by Bartoli et al. (2016), based on a different form of optimization which includes, in the solution presentation, some domain knowledge concerning the shape of the tiles.

Acknowledgments

The experimental evaluation of this work has been done on Amazon AWS within the "AWS Cloud Credits for Research" program.

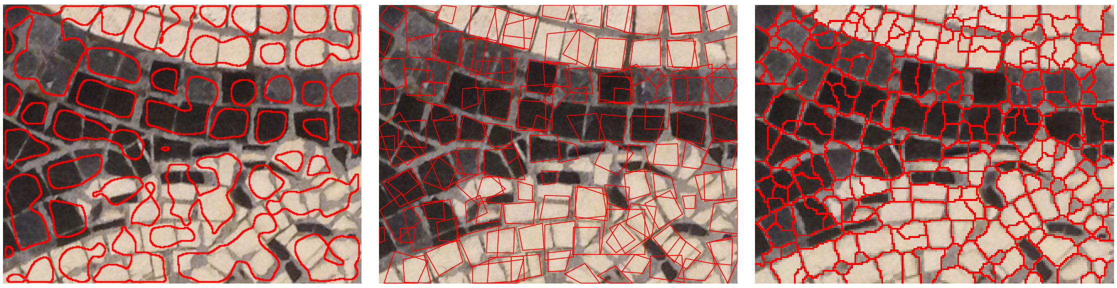

(a) U-net (b) GA (c) TOS

Figure 2: Example of segmentation of image 11 overlapped on the original image with the three methods.

REFERENCES

Assael, Y., Sommerschield, T., and Prag, J. (2019). Restoring ancient text using deep learning: a case study on greek epigraphy. *arXiv preprint arXiv:1910.06262*.

Bartoli, A., Fenu, G., Medvet, E., Pellegrino, F. A., and Timeus, N. (2016). Segmentation of mosaic images based on deformable models using genetic algorithms. In *International Conference on Smart Objects and Technologies for Social Good*, pages 233–242. Springer, Springer.

Benyoussef, L. and Derrode, S. (2011). Analysis of ancient mosaic images for dedicated applications. In Stanco, F., Battiato, S., and Gallo, G., editors, *Digital Imaging for Cultural Heritage Preservation: Analysis, Restoration, and Reconstruction of Ancient Artworks*. CRC Press.

Çiçek, Ö., Abdulkadir, A., Lienkamp, S. S., Brox, T., and Ronneberger, O. (2016). 3d u-net: learning dense volumetric segmentation from sparse annotation. In *International conference on medical image computing and computer-assisted intervention*, pages 424–432. Springer.

Comes, R., Buna, Z., and Badiu, I. (2014). Creation and preservation of digital cultural heritage. *Journal of Ancient History and Archaeology*, 1(2).

Falk, T., Mai, D., Bensch, R., Çiçek, Ö., Abdulkadir, A., Marrakchi, Y., Böhm, A., Deubner, J., Jäckel, Z., Seiwald, K., et al. (2019). U-net: deep learning for cell counting, detection, and morphometry. *Nature methods*, 16(1):67.

Fazio, L., Brutto, M. L., and Dardanelli, G. (2019). Survey and virtual reconstruction of ancient roman floors in an archaeological context. *International Archives of the Photogrammetry, Remote Sensing and Spatial Information Sciences*, 42(2/W11).

Fenu, G., Jain, N., Medvet, E., Pellegrino, F. A., and Pilutti Namer, M. (2015). On the assessment of segmentation methods for images of mosaics. In *International Conference on Computer Vision Theory and Applications-VISAPP*, volume 3, pages 130–137. SciTePress, SciTePress.

Kingma, D. P. and Ba, J. L. (2015). Adam: A method for stochastic optimization. In *Proceedings of the 3rd International Conference on Learning Representations (ICLR)*.

Kohl, S., Romera-Paredes, B., Meyer, C., De Fauw, J., Ledsam, J. R., Maier-Hein, K., Eslami, S. A., Rezende, D. J., and Ronneberger, O. (2018). A probabilistic u-net for segmentation of ambiguous images. In *Advances in Neural Information Processing Systems*, pages 6965–6975.

Monti, M. and Maino, G. (2011). Image processing and a virtual restoration hypothesis for mosaics and their cartoons. In *International Conference on Image Analysis and Processing*, pages 486–495. Springer.

Neumüller, M., Reichinger, A., Rist, F., and Kern, C. (2014). 3d printing for cultural heritage: Preservation, accessibility, research and education. In *3D Research Challenges in Cultural Heritage*, pages 119–134. Springer.

Ronneberger, O., Fischer, P., and Brox, T. (2015). U-net: Convolutional networks for biomedical image segmentation. In *International Conference on Medical image computing and computer-assisted intervention*, pages 234–241. Springer.

Vincent, L. and Soille, P. (1991). Watersheds in digital spaces: an efficient algorithm based on immersion simulations. *IEEE Transactions on Pattern Analysis and Machine Intelligence*, 13(6):583–598.

Youssef, L. B. and Derrode, S. (2008). Tessella-oriented segmentation and guidelines estimation of ancient mosaic images. *Journal of Electronic Imaging*, 17(4):043014.

Zhang, Z., Liu, Q., and Wang, Y. (2018). Road extraction by deep residual u-net. *IEEE Geoscience and Remote Sensing Letters*, 15(5):749–753.